Spatial distribution of electric field measurement system: straight characterization of one or more original electric field sources in association with a new triaxial sensor

Matthieu Roblin, Didier Robbes, Gilles Allégre, Matthieu Denoual, Olivier Mareschal

High accuracy electric field measurement system for characterization of both new tri-axial sensor and original electric field sources

Matthieu Roblin, Didier Robbes, Gilles Allègre, Matthieu Denoual, Olivier Mareschal

***Abstract*—A new tri-axial capacitive based electric field sensor is presented with a sensitivity of $1\,\mathrm{mV}\cdot\mathrm{m}^{-1}/\sqrt{\mathrm{Hz}}$ and a $16\,\mathrm{bit}$ dynamic range in the frequency range $100\,\mathrm{Hz}$ - $10\,\mathrm{kHz}$. The sensor is integrated in a 2D scanning setup and used to map simultaneously the three components of the electric field generated by original electric field sources composed of several conductive spheres. These sources are designed with conical support and contact so that they can be assimilated to point charges and can be arranged under different phase configurations to generate monopolar to multipolar electric fields. The measured electric field images are compared to images calculated with an analytical model using the method of image charges. The agreement between measured electric field images and model validates both the sources and the sensor which open the door to application such as the detection of non-conductive buried object.**

***Index Terms*—electric field sensor, electric field source, imaging, 2D scanning, method of image charges**

I. Introduction

THE measurement of stationary and slowly varying electric field (EF) has been investigated in several domains of research with different types of EF sensors [1], [2], [3]. EF sensors have been used in atmospheric science to study and predict meteorological phenomena such as lightning storms [4], [5], [6], [7] or sand storms [8] and are now part of payloads for solar system exploration missions [9]. In industrial applications, EF sensors can be used to prevent electrostatic discharge (ESD) during electronic manufacturing processes [10] or as online diagnostics for non-contact detection of internal defects in non-ceramic insulators [11], [12]. EF under power lines have also been investigated to understand potential health effects from exposure to EM fields [13], [14], [15] or to detect ice accretion on high power electric cables [16]. In medical applications, EF sensors have been developed for biometric measurement such as non-contact electroencephalogram and electrocardiogram with electrode that capacitively couples to the skin to avoid using electrically-conductive gels between the sensor and scalp [17], [18]. EF probes have also been used to study biological systems such as tissues or cells [19] or biological species with electric sensory abilities such as fishes [20].

These multiple applications generally require non-contact measurements but other requirements are sometimes needed such as small dimension, wide bandwidth, large dynamic range, compatibility with liquids and gases, full 3D vectorial detection, capability of measuring electric fields up to the electric breakdown of air. For this reason, different types of EF sensors have been studied and developped [1], [21]. EF sensors may be classified into two categories: mechanical EF sensors (rotating and vibrating electric field mill, MEMS) and non-mechanical EF sensors (electro-optical, electric fluxgate, ferroelectric capacitors, capacitive).

The rotating field mill is one of the best known DC EF sensors [4], [5], [13], [15], [22]. The incident field is repeatedly chopped by an electrically grounded shutter which generate a measurable AC field and whose amplitude is proportional to the incident DC field. An alternative and more compact geometry has been presented consisting of a cylindrical rotating sensor capable of measuring two components of the EF [8]. With the development of micro-fabrication technology MEMS, the concept of the macroscopic field mill has been miniaturized. The MEMS field mill use a vertically or laterally vibrating perforated grounded shutter to periodically shield the underlying sense electrodes from the incident DC field [6], [7], [10], [12], [16] and a tri-axial version has been presented [23].

Non-mechanical EF sensors have also been developed such as optical sensors based on the Pockels effect through the modification of the indices of refraction of an electro-optic crystal by the electric field. Probed by a low noise laser beam, information about magnitude and phase are encoded in the polarization state of the laser beam and two components of the EF can be recovered [2], [19], [21], [24]. Fluxgate electric field meters have also been investigated [25] as well as sensors based on a ferroelectric capacitor acting as a nonlinear active dynamic element where the EF is converted into a perturbation on the polarization state of a ferroelectric material [26]. A last category are the capacitive sensors that combine one or an array of electrodes and can measure the displacement currents induced by time-varying EF and recover the electric potential and the electric field with a high sensitivity [18], [20], [27], [28].

Despite several sensors, EF measurement has remained a research field with some exceptions for niche markets, unlike magnetic field measurement with multiple magnetic field sensors (induction coils, Hall and magnetoresistance sensors, fluxgates and SQUIDs), some of which are now widely used, particularly for medical [29] and industrial applications [30] and easily accessible to the general public. This imbalance between magnetic and electric field sensors can be attributed to the ability of the EF to interact with any surrounding objects, conductive or not, which makes the design of EF sensors challenging (grounded sensors distort the EF in their vicinity producing large errors and multi-axial sensors suffer from

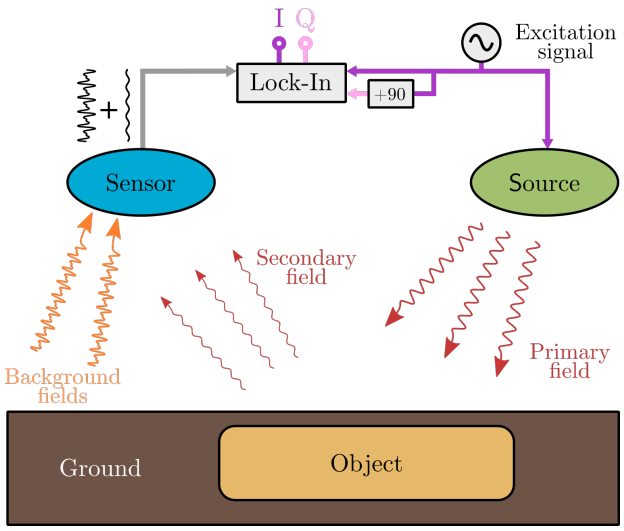

Fig. 1. Schematic of lock-in detection system (in-phase I, quadrature Q) based on the measurement of a secondary field generated by an object placed in a primary field.

cross-axis coupling interference) but opens new possibilities.

A long-term objective of this research work is to develop a detection system in the frequency range 100 Hz - 100 kHz using the electric field to detect buried objects or defects in objects without the constraint for the object to be a conductive material as it is the case for eddy current testing techniques (ECT) based on the magnetic field that are used in industry applications as non-destructive techniques to detect defects in conductive material and to control the quality of components [30].

Such a detection system requires an excitation source to generate an EF (the primary field), controlled and configurable, at a specific frequency and a high-dynamic sensor that can be a single well oriented EF sensor as in [31] or a three directional EF sensor to fully characterize the EF response (figure 1). The interaction of this primary field with a nearby object generates an induced secondary field. The induced field depends on the shape of the object as well as on the physical properties (permittivity, conductivity) of both the object and its surrounding medium at the excitation frequency [20]. The sensor detects the primary and the secondary fields but also any background electric fields (such as the line electric field produced by surrounding electronic devices). Because the secondary field may be much smaller compared to background fields, standard lock-in technique is required to extract the signal of interest. In-phase (I) and quadrature (Q) signals, recovered from the lock-in amplifier, contain information related to the shape, the distance and the material composition of the object. As in magnetics, the shape information and the physical properties are included within both the in-phase and quadrature part of the signal.

To get a controlled and configurable EF source as well as a high dynamic 3D EF sensor, an original EF source and a new concept of EF sensor have been developed that are presented in this paper. The EF source has been designed so that it can be assimilated to a point charge. Several of these sources can then be arranged under different phase configurations to generate monopolar to multipolar EF sources. Thanks to the spherical geometry of the source, the generated EF can be calculated by an analytical model that is also presented in the paper. The sensor is a triaxial capacitive based sensor [32] (figure 2) working in the low frequency range 100 Hz - 10 kHz with a high sensitivity of $1\,\mathrm{mV}\cdot\mathrm{m}^{-1}/\sqrt{\mathrm{Hz}}$ and a 16-bit dynamic range. To characterize and validate these two new elements, a specific experimental setup has been implemented.

The paper is organized as follows:

- the section II presents the measurement principle;
- the section III presents the complete experimental setup with the EF source, the 3D EF sensor and the XY scanning test bench;
- the section IV presents the analytical model;
- the section V presents different measurements and their comparison with the model.

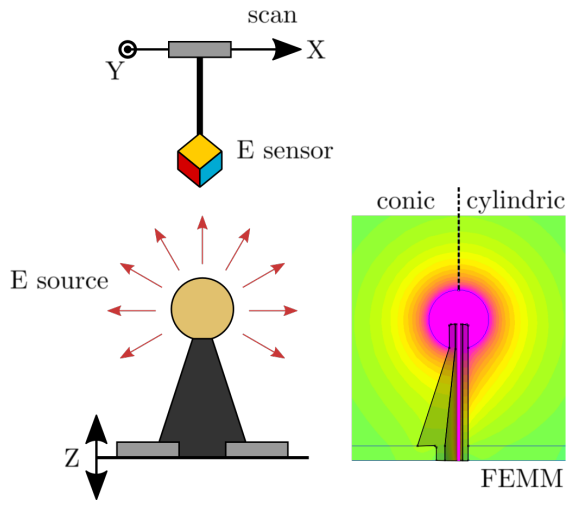

Fig. 2. (left) Side-view of an EF sensor scanning above an EF source; (right) FEMM simulations of the electric potential map of a sphere with a support body having a conical (left part) or a cylindrical (right part) geometry.

II. Principle

To have a well-controlled electric field, it can be wise to use a source as close as possible to the ideal case of the point charge with a purely radial emission. In last century electrostatics experiments, the spherical shape has been repeatedly used to build EF sources. Indeed, the EF emitted by a standalone sphere (at fixed potential) is equivalent to an EF emitted by a point charge. However, for pratical reason, a structure is required to support the sphere and precaution are needed to avoid this support distorting the expected radial EF. An innovative solution is to use a support structure with a conical shape [27] (figure 2) made in conductive material and designed so that the outer surface is parallel to the theoretical EF of an unique sphere meaning that the equipotential lines are perpendicular to the outer surface and concentric around the sphere. Also the wire used to supply electrical charges to the sphere can be routed inside the support body to avoid any distorsion from the EF of the wire. If the cone structure was infinitely long, the source would be equivalent to a standalone

sphere. For practical reason, it is not the case but a cone length several times longer than the radius of the sphere achieves the expected accuracy. Two FEMM simulations of a sphere at fixed potential and supported by a conical (left part) or a cylindrical body (right part) are displayed in figure 2 (right). With the cylindrical body, the EF is pyriform whereas with the conical body, the EF stays spherical. For a unique source, the EF is equivalent to a point charge. In the case of two sources (or more), when the two spheres get closer, image charges appears because each sphere stays at fixed potential. The EF can be calculated analytically using a model based on the method of image charges. Under different phase excitations, monopolar to multipolar EF can be generated.

In a similar way for the sensor, the objective is to propose a tri-axial EF sensor designed to minimize its own influence on the measurement itself. The sensor, developed and integrated at the laboratory (figure 3), is based on a concept that was initially implemented in a mono-axial design [27] and then transposed to three dimensions. The concept of the mono-axial probe is derived from a capacitive structure consisting of a pair of electrodes which, when placed in an external EF, generates a measurable potential difference directly related to the EF component in the orthogonal direction to the electrodes.

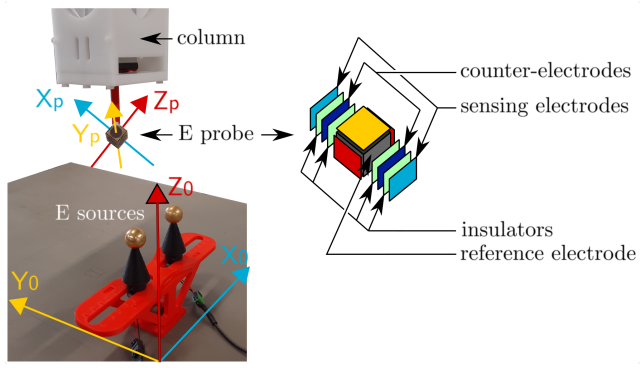

Fig. 3. (left) Photography of the tri-axial probe (20 mm wide) during the scan above two sources; (right) exploded view of the tri-axial EF sensor along Xp direction.

These two new elements are characterized with a XY scanning test bench. The sensor is mounted on the scanning system and is moved in a plane above different configurations of EF spherical sources. Images of the three EF components are then measured and compared with the theoretical components evaluated using an analytical model based on the method of image charges [33].

III. Experimental Setup

A. Electric field source description

The EF source is composed of several brass spheres supported by conductive structures made of conical electrically active polymer with electrical resistivity in the range of 10^3 - 10^5 Ω·cm. Sine voltages of several volts in amplitude are applied on the spheres in the frequency range 100 Hz - 10 kHz thanks to electrical wires passing through their support body and connected to the spheres. The sinusoidal excitation signals are generated by a quad digital to analog converter (DAC) including complex waveform generation with a Direct Digital Synthesizer (DDS) AD9106 (figure 4). The DDS has a 12-bit output with a single frequency for all four DACs and independent programmable phase shift outputs for each of the four DACs. Two outputs ①, ② are used to supply as reference signals for lock-in amplifiers and the two others ③, ④ as excitation signals. To avoid phase shifts between measurement channels (E_{Xp}, E_{Yp} and E_{Zp}) and the two reference channels, the same band pass filters are used. Reference sine signals are converted to square signals with comparators before being supplied to lock-in amplifiers (LIA).

Depending on the number of spheres and of DAC phases, several excitation modes are possible: monopolar to multipolar modes.

Figure 4 illustrates the case of a dipolar excitation with two spheres where DDS3 and DDS4 are in phase opposition.

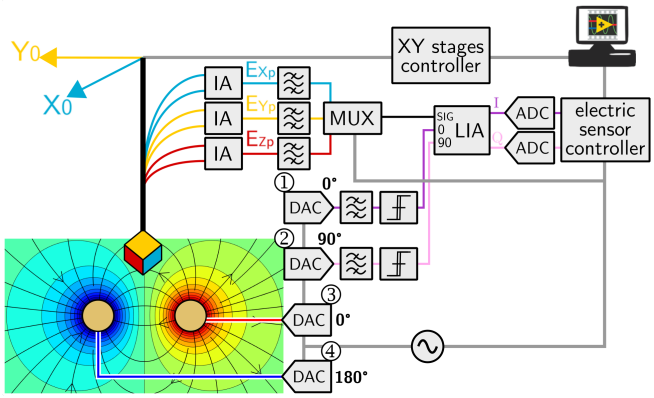

Fig. 4. Sketch-view of the measurement setup.

B. Description of the electric field sensor and its conditioning electronics

The transition from the monoaxial [27] to the triaxial configuration (figure 3) led to the construction of a 20 mm wide cube built on an arrangement of three orthogonal pairs of sensing electrodes. However, such a construction suffers from deviations due to the influence between the orthogonal electrodes. It is possible to minimize the effect of this inter-electrodes crosstalk by using the guard ring technique by splitting each electrode into a pair of sensing and counter-electrodes [32]. The purpose of the counter-electrode is to reproduce the potential variations of the sensing electrode. Each pair of sensing electrode/counter-electrode is isolated from the other pairs by a closed shielding set at the reference potential - the reference electrode - to avoid the diffusion of the potential inside the sensor's cavity. At last, it is possible to use a counter-reaction effect by connecting each sensing electrode to the counter-electrode on the opposite side of the cube leading to a higher dynamic.

The cube is held at one corner by a cylindric tube aligned with the cube diagonal, to ensure a ternary symmetry. The wires from the sensing electrodes are routed inside the cubic body and then through the tube to reach the signal conditioning circuits disposed inside the column. The three measurement

axis of the probe - Xp, Yp and Zp - are normal to the faces of the cube and chosen by convention in the direction of the tube (figure 3).

The principle of the signal conditioning is multiplexed lock-in detection (figure 4). The two signals from each pair of electrodes are sent to an instrumentation amplifier (IA). Each channel (E_{Xp}, E_{Yp} and E_{Zp}) is filtered and sent to a multiplexer (MUX) which redirects them sequentially to two LIA locked in-phase and in-quadrature with respect to the excitation signal applied to the sources. The multiplexing limits the acquisition rate to 3 Hz.

Signals from LIAs are digitized by a 24-bit quad ADC board ADS131A04 and stored.

The sensor presented in this paper has a sensitivity of $1\,\mathrm{mV}\cdot\mathrm{m}^{-1}/\sqrt{\mathrm{Hz}}$ and a 16-bit dynamic range in the frequency range 100 Hz - 10 kHz. This sensor is thus able to mesure simultaneously the full vectorial electric field with good performances comparable to electro-optic sensors [24] and a better dynamic range compared to MEMS [7] while using conventional mechanical and electronic components that do not require integration in cleanroom facilities.

C. Description of the 2D scanning setup

The sensor and the signal conditioning circuits are integrated inside a square column with the probe tip passing through the bottom of the column (figure 5). The column is vertically suspended from a system of translation rails mounted on a cage structure. The translation system consists of a linear toothed belt axis (Y-axis) whose ends rest on two orthogonal rails (X-axis). The rails are driven by stepper motors. The column can cover an area of $150\,\mathrm{cm}\times 150\,\mathrm{cm}$.

The sources excitation, the XY scanning system and the measurement acquisition are controlled by a dedicated LabVIEW software.

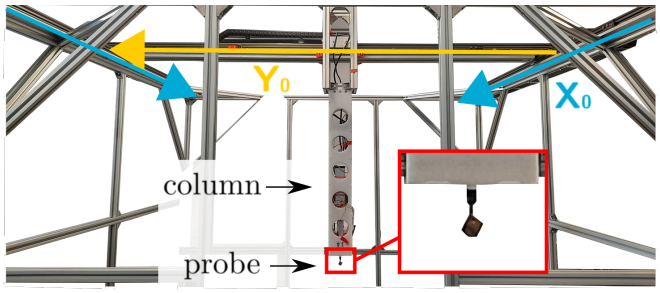

Fig. 5. Photography of the XY scanning cage structure with the column centered in the middle of the cage and the EF probe at its tip.

IV. Simulations

In the case of multiple spherical sources close to each other, considering that each sphere is a point charge and applying the superposition principle is inaccurate. For that reason, an analytical model based on the method of image charges [33], [34] has been developed to calculate the spatial distribution of the EF generated by a system of conducting spheres.

An image charge (or electrical image) is defined by Maxwell as "an electrified point or system of points on one side of a surface which would produce on the other side of that surface the same electrical action which the actual electrification of that surface really does produce".

In the case of a system of conducting spheres at fixed potential, a set of image charges inside the spheres must be found so that the surfaces of the spheres are equipotential.

For a single sphere, a unique central point charge q can be considered equal to $4\pi\epsilon_0 aV$ with a the radius of the sphere and V the potential applied on the sphere.

For several spheres, if the superposition principle is applied by replacing each sphere to a single point charge, the field distribution is distorted and the surfaces of the spheres are no longer equipotential.

In order to make them equipotential, it is necessary to add iteratively several orders of image charges where each order is calculated taking into account all the charges calculated at the previous orders. At each order, the number of new image charges is given by the formula: $S(S-1)^N$ (S: number of spheres, N: order) which increases rather quickly as the number of spheres gets higher (236 196 charges at order 10 for four spheres).

The electric potential can then be written exactly as an infinity of nested sums of image charges potentials where each new sum is an additional order of image charges (equation 1).

$$V(\vec{r}) = \frac{1}{4\pi\epsilon_0}\sum_{i=1}^{S}\left(\frac{q_i}{|\vec{r}-\vec{r}_i|}+\sum_{\substack{j=1\\ j\neq i}}^{S}\left(\frac{q_{ij}}{|\vec{r}-\vec{r}_{ij}|}+\sum_{\substack{k=1\\ k\neq j}}^{S}\left(\frac{q_{ijk}}{|\vec{r}-\vec{r}_{ijk}|}+\ldots\right)\right)\right) \quad (1)$$

where:

$$q_i = 4\pi\epsilon_0 a_i V_i,\quad q_{ij} = -\frac{a_i}{|\vec{r}_i-\vec{r}_j|}q_j,\quad q_{ijk} = -\frac{a_i}{|\vec{r}_i-\vec{r}_{jk}|}q_{jk}$$

$$\vec{r}_{ij} = \vec{r}_i - a_i^2\frac{\vec{r}_i-\vec{r}_j}{|\vec{r}_i-\vec{r}_j|^2},\quad \vec{r}_{ijk} = \vec{r}_i - a_i^2\frac{\vec{r}_i-\vec{r}_{jk}}{|\vec{r}_i-\vec{r}_{jk}|^2}$$

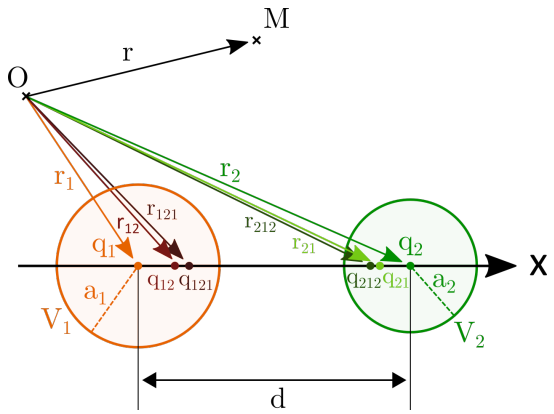

Fig. 6. Order 2 image charges of two conductive spheres.

We notice that the number of indices associated to image charges increases with the order. If we consider the case of two spheres (figure 6), two new image charges are added at

each order, q_1 and q_2 at order 0, q_{12} and q_{21} at order 1, q_{121} and q_{212} at order 2, and so on.... q_{212} is an image charge on sphere 2 of q_{12} which itself is an image charge on sphere 1 of q_2.

The truncation of the equation (1) at a specific order is then an approximation and the choice of the order of the truncation will depend on the degree of accuracy required. The impact of the truncation can be evaluated by calculating the potential at any point on the perimeter of the sphere. Let us take the case of two spheres of radius $a_1 = a_2 = 50\,\mathrm{mm}$, separated by a distance $d = 50\,\mathrm{mm}$, with potentials fixed at $V_1 = V_2 = 1\,\mathrm{V}$. The calculation of the potential along the perimeter of the sphere 1 in the plane passing through the center of the two spheres is illustrated figure 7b and the deviation from the theoretical value figure 7c. The potential maps are shown at order 0 and at order 5 (figure 7a). At order 0, the 1 V equipotential (white outline) is far from the surfaces of the spheres (black disks) leading to a 25% error. Adding image charges brings it closer and reduces the error down to 0.01% at order 5.

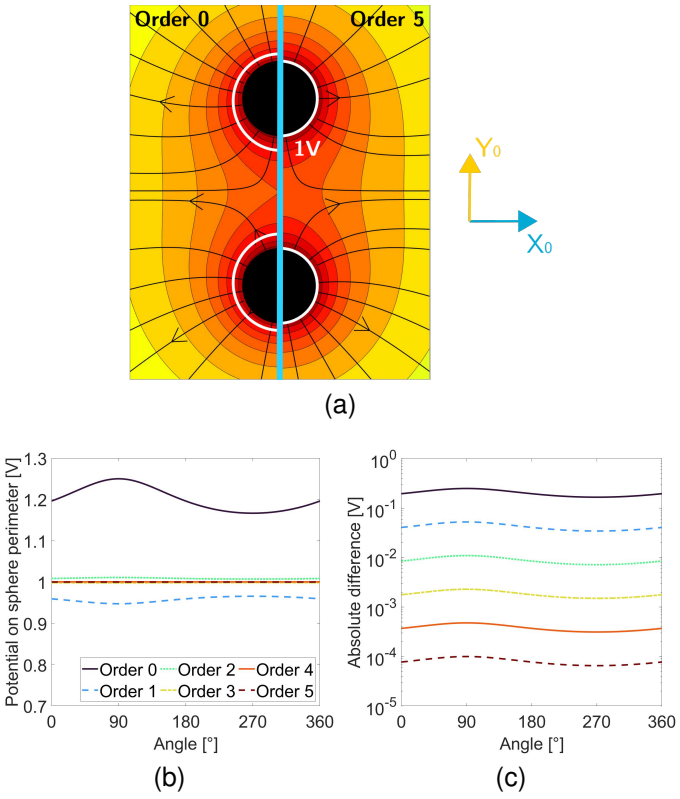

Fig. 7. Potential map for two spheres of radius 10 mm, separated by 50 mm at potential 1 V calculated in a plane passing by the center of the two spheres: a) Comparison of potential maps at order 0 (left) and 5 (right); b) Potential along the perimeter of sphere 1; c) Deviation from the theoretical value of the potential along the perimeter.

From the electric potential, the three components of the EF can be calculated (as illustrated in the next section) and compared to the tri-axial sensor measurements.

All of the image processing steps as well as the model of the conductive spheres have been implemented in the Matlab environment.

V. Results

Using spherical sources that can be approximated as point-like sources allows to easily combine several of them in various monopolar or multipolar configurations. The calculation of the generated EF can be done with the developed simulation tool and then compared with measured EF images acquired on the experimental setup.

The simplest configuration with at least one symetry with respect to the sensor is two spheres excited in phase (figure 3). In this case, the EF in an horizontal area above and between the sources in the X_0Y_0 plane is mainly directed in the vertical direction Z_0 .

To switch the orientation of the EF to an horizontal direction, the two spheres can be excited in phase opposition to get a dipolar excitation. In this case, the EF in an horizontal area above and between the sources in the X_0Y_0 plane is mainly directed in the horizontal direction X_0. To extend and homogenize the area where the EF is horizontal, four spheres can be used in dipolar configuration.

Two series of EF measurements are presented and compared to the analytical model:

1) A measurement above two spheres (example on figure 3) of 10 mm radius separated by a distance of 50 mm (distance between the centers of the spheres) and excited by in-phase sinusoidal signals at 1 kHz with an amplitude of 1.1 V (corresponding to an EF of $110\,\mathrm{V{\cdot}m^{-1}}$ close to the surface of the sphere).
2) A measurement above four spheres of 10 mm radius distributed at the four corners of a 50 mm square and supplied two by two with opposite polarity (YZ anti-symmetry plane) at 1 kHz with an amplitude of 1.1 V.

Because the environment consists in spherical sources surrounded by air, no information is contained into the quadrature part Q of the signal. For this reason, only in-phase results are presented.

The sensor is scanned in an X_0Y_0 plane at a height Z_0 = 55 mm with respect to the plane passing by the center of the spheres. 81 successive scans are done in the +Y direction. Three images of 84×81 pixels ($24.9\,\mathrm{cm} \times 33.2\,\mathrm{cm}$) are recorded corresponding to the three field components in the directions Xp, Yp and Zp associated with the sensor probe (figure 3) and in phase with respect to the excitation signals.

The images are cleaned using a median filter and then are projected from the sensor reference frame (Xp, Yp, Zp) to the setup reference frame (X_0, Y_0, Z_0) (figure 8).

To compare with the measurements, the expected electric potential maps are calculated with the model of the conducting spheres at order 5 (figure 9) and the three EF components are deduced from the gradient of the potential maps. Figure 10 shows the three EF components measured (left column) and calculated (middle column).

To allow the comparison between measurement and model, a spatial interpolation is applied on measured images so that the images have the same dimensions. Then, an image

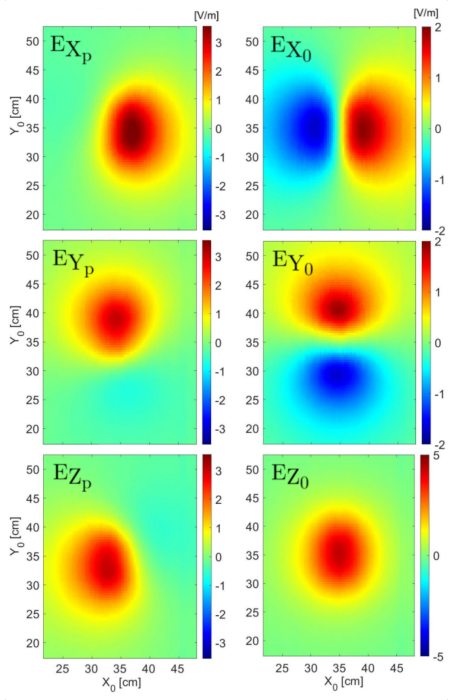

Fig. 8. Angular projection of the three EF components of series of in-phase measurement n°1 from the reference frame of the sensor (left) to the reference frame of the test bench (right).

registration step[1] is applied to correct the misalignement in positioning and orientation of the spheres with respect to the scanning directions (rigid transformation: translation and rotation). Finally, for each component, the ratio of the difference between measurement and model divided by the norm of the calculated EF is displayed in the right column of figure 10.

To extract more quantitative values from these image comparisons, the percentage of the covered area (cv) contained within $\pm 5\%$ error (white areas) is evaluated and the average of the absolute difference (rel) for each EF components relative to the norm of the theoretical EF is calculated in these areas. A grey mask is applied to ignore the areas where the norm of the EF is lower than 10% of the maximum. A good agreement is observed for the configuration 1 (2 spheres) for the E_X component where a relative difference 2.1% with a $\pm 5\%$ area covering 85% of the image. Higher deviations are observed in the configuration 2 (4 spheres) particularly for the E_Z component.

VI. Discussion

The observed discrepancies are potentially caused by a combination of different sources of error such as the relative spatial and angular positioning between the EF sources, the probe and the XY scanning system or the imperfections of this first prototype with faces not perfectly orthogonals (measured deviations of the order of 1°). These multiple factors of uncertainties find themselves intertwinded and are only partially compensated by the processing steps. To reduce the number of free parameters currently existing on the setup, several improvements are foreseen such as the realization of a new probe with a better control of the dimensions or the addition of a LIDAR to improve the control of the positioning of the different elements.

[1]Image registration is defined as a process that overlays two or more images from various imaging equipment or sensors taken at different times and angles, or from the same scene to geometrically align the images for analysis [35].

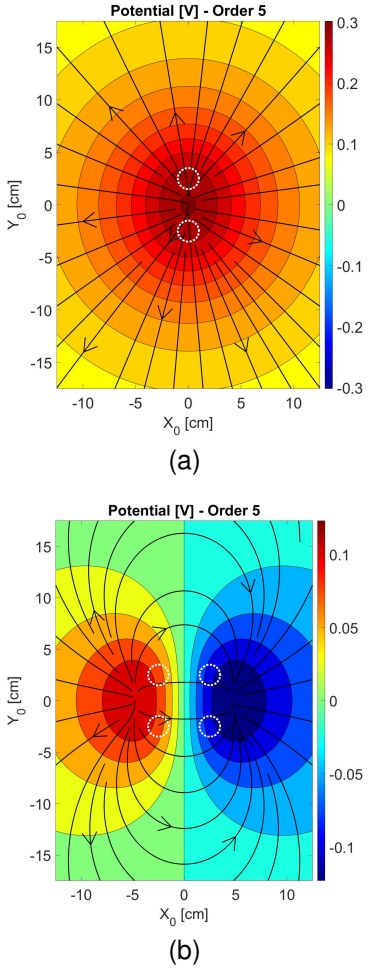

Fig. 9. a) Potential map in an X_0Y_0 plane in $Z = 55\,\mathrm{mm}$ above a monopolar system of two spheres of radius $10\,\mathrm{mm}$ separated by a distance of $50\,\mathrm{mm}$ at potentials $+1.1\,\mathrm{V}$; b) Potential map in an X_0Y_0 plane in $Z = 55\,\mathrm{mm}$ above a dipolar system of four spheres of radius $10\,\mathrm{mm}$ distributed at the four corners of a square of $50\,\mathrm{mm}$ side and supplied in phase opposition by pair at potentials of +/- $1.1\,\mathrm{V}$. Spheres are symbolized by white dotted circles.

VII. Conclusion

One of the long-term objectives of this research work is to develop an electric field based detection system in the low frequency range with the ability to detect buried objects or detect defects in materials as in eddy current testing techniques but compatible with non-conductive materials. To build this system, a new triaxial cubic EF sensor, original EF spherical sources and a XY scanning test bench have been developped and presented in this paper.

The new tri-axial EF capacitive based sensor sensor has been built using conventional mechanical and electronic components that do not require access to cleanroom facilities. The sensor has a sensitivity of $1\,\mathrm{mV \cdot m^{-1}/\sqrt{Hz}}$ and a $16\,\mathrm{bit}$

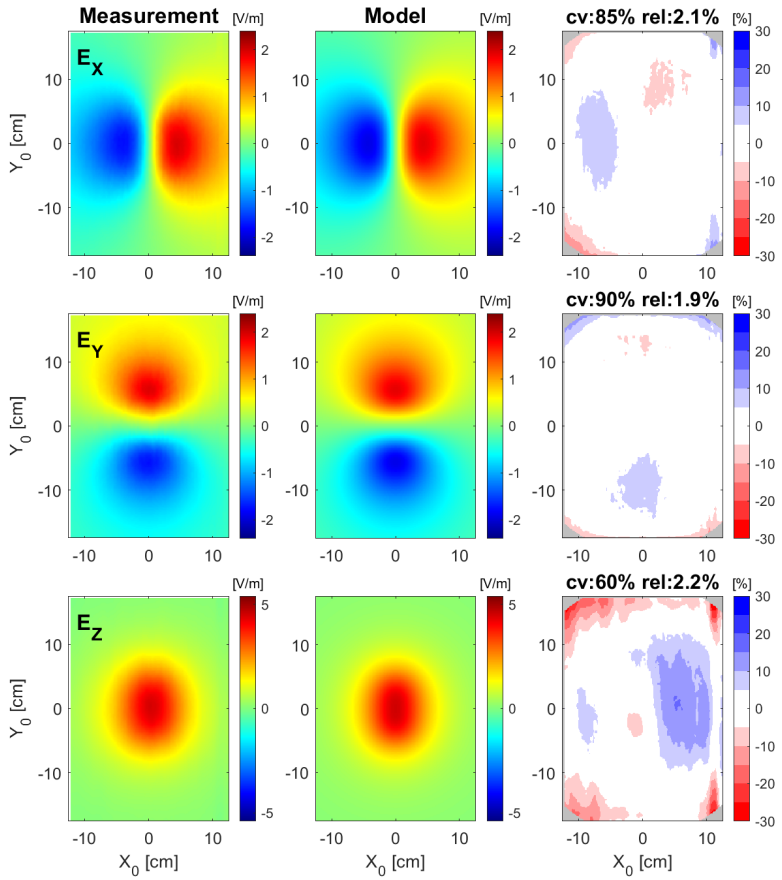

(a)

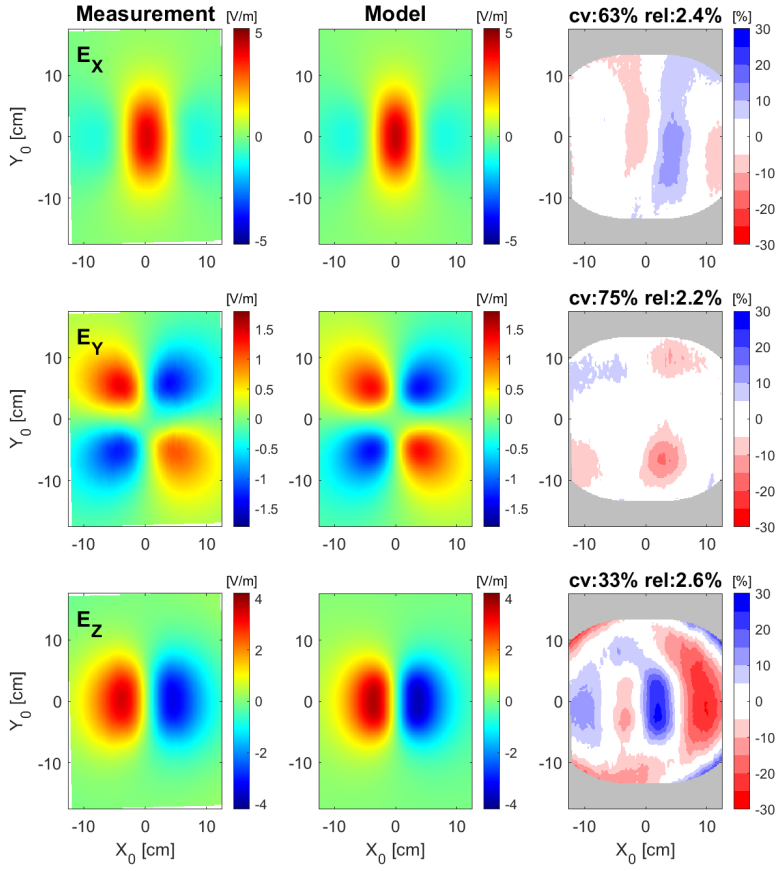

(b)

Fig. 10. Electric field maps of the three components of the EF for the measurement (left column), the model (middle column) and the relative difference (right column) associated to the two series of measurement: a) Two spheres in monopolar configuration; b) Four spheres in dipolar configuration.

dynamic range in the frequency range 100 Hz - 10 kHz and is able to mesure simultaneously the full vectorial electric field with performances comparable to electro-optic sensors [24] and a better dynamic range than MEMS [7].

EF sources composed of spherical spheres mounted onto original conical support structures have been designed and fabricated. Theses sources can be individually approximated as point charges and combined to generate monopolar or multipolar EF fields. An analytical model has been implemented to predict the EF generated by any arrangements of these sources.

The sensor mounted onto a 2D scanning setup is used to map the EF generated by two arrangements of EF sources, with two sources in monopolar configuration and four sources in dipolar configuration. The measured EF images have been compared to calculated images and a good consistency has been obtained allowing to validate both the new sources and the sensor.

By fixing EF sources directly on the column moving along with the EF sensor, the next objective will be to detect non-conductive buried object. Setup improvements are planned to increase the dynamic range, the acquisition rate and to reduce the noise. Probe miniaturisation is considered and a new signal conditioning with one lock-in amplifier per axis is under development.

REFERENCES

[1] H. Kirkham, "On the measurement of stationary electric fields in air," pp. 524 – 525, 02 2002.

[2] R. Miles, T. Bond, and G. Meyer, "Report on non-contact DC electric field sensors," 01 2009.

[3] D. Taylor, "Measuring techniques for electrostatics," *Journal of Electrostatics*, vol. 51-52, pp. 502–508, 2001. Electrostatics 2001: 9th International Conference on Electrostatics.

[4] L. Raymond, B. Jeffrey, C. Bailey, D. Mach, M. Stewart, and H. Christian, "Study of triggered lightning: The airborne field mill program," in *10th Annual International Symposium on Geoscience and Remote Sensing*, pp. 1901–1904, 1990.

[5] J. Singye, K. Masugata, T. Murai, I. Kitamura, and K. Kontani, "Thunderstorm tracking system using neural networks and measured electric fields from few field mills," in *2005 IEEE International Symposium on Circuits and Systems*, pp. 5126–5129 Vol. 5, 2005.

[6] P. Yang, B. Chen, X. Wen, C. Peng, S. Xia, and Y. Hao, "A novel MEMS chip-based atmospheric electric field sensor for lightning hazard warning applications," in *2015 IEEE SENSORS*, pp. 1–4, 2015.

[7] W. Xiaolong, P. Yang, C. Zhaozhi, C. Peng, L. Yutao, and W. Shuang, "MEMS-based electric field sensor with environmental adaptability consideration and its application in the near-ground atmosphere," *Journal of Physics: Conference Series*, vol. 1775, p. 012003, jan 2021.

[8] N. O. Renno, J. F. Kok, H. Kirkham, and S. Rogacki, "A miniature sensor for electrical field measurements in dusty planetary atmospheres," *Journal of Physics: Conference Series*, vol. 142, p. 012075, dec 2008.

[9] R. Lorenz, E. Turtle, J. Barnes, M. Trainer, D. Adams, K. Hibbard, C. Sheldon, K. Zacny, P. Peplowski, D. Lawrence, M. Ravine, T. McGee, K. Sotzen, S. MacKenzie, J. Langelaan, S. Schmitz, L. Wolfarth, and P. Bedini, "Dragonfly: A rotorcraft lander concept for scientific exploration at Titan," *Johns Hopkins APL Technical Digest (Applied Physics Laboratory)*, vol. 34, pp. 374–387, 10 2018.

[10] X. Chen, C. Peng, H. Tao, C. Ye, Q. Bai, S. Chen, and S. Xia, "Thermally driven micro-electrostatic fieldmeter," *Sensors and Actuators A: Physical*, vol. 132, no. 2, pp. 677–682, 2006.

[11] I. Ramirez-Vazquez, R. Hernandez-Corona, and G. Montoya-Tena, "Diagnostic of nonceramic insulators aged in a salt fog chamber by using electric field sensor," in *Conference Record of the 2004 IEEE International Symposium on Electrical Insulation*, pp. 471–474, 2004.

[12] C. Peng, P. Yang, S. Liu, H. Zhang, K. Feng, and S. Xia, "Detecting internal defect of non-ceramic insulators using a novel micromachined electric field sensor," in *2011 IEEE 24th International Conference on Micro Electro Mechanical Systems*, pp. 561–564, 2011.

[13] P. S. Maruvada, R. Dallaire, and R. Pedneault, "Development of field-mill instruments for ground-level and above-ground electric field measurement under HVDC transmission lines," *IEEE Transactions on Power Apparatus and Systems*, vol. PAS-102, no. 3, pp. 738–744, 1983.

[14] A. Johnston and H. Kirkham, "A miniaturized space-potential DC electric field meter," *IEEE Transactions on Power Delivery*, vol. 4, no. 2, pp. 1253–1261, 1989.

[15] Y. Cui, H. Yuan, X. Song, L. Zhao, Y. Liu, and L. Lin, "Model, design, and testing of field mill sensors for measuring electric fields under high-voltage direct-current power lines," *IEEE Transactions on Industrial Electronics*, vol. 65, no. 1, pp. 608–615, 2018.

[16] P. Yang, C. Peng, H. Zhang, S. Liu, D. Fang, and S. Xia, "A high sensitivity SOI electric-field sensor with novel comb-shaped microelectrodes," in *2011 16th International Solid-State Sensors, Actuators and Microsystems Conference*, pp. 1034–1037, 2011.

[17] T. J. Sullivan, S. R. Deiss, and G. Cauwenberghs, "A low-noise, non-contact EEG/ECG sensor," in *2007 IEEE Biomedical Circuits and Systems Conference*, pp. 154–157, 2007.

[18] E. Rendon-Morales, R. J. Prance, H. Prance, and R. Aviles-Espinosa, "Non-invasive electrocardiogram detection of in vivo zebrafish embryos using electric potential sensors," *Applied Physics Letters*, vol. 107, no. 19, p. 193701, 2015.

[19] P. Jarrige, N. Ticaud, S. Kohler, R. O'Connor, L. Duvillaret, G. Gaborit, D. Arnaud-Cormos, and P. Leveque, "Electro-optic probe adapted for bioelectromagnetic experimental investigations," *IEEE Transactions on Instrumentation and Measurement*, vol. 61, pp. 2051–2058, 07 2012.

[20] B. Rasnow, "The effects of simple objects on the electric field of apteronotus," *Journal of Comparative Physiology A*, vol. 178, pp. 397–411, 03 1996.

[21] Z. Gao, Z. Yu, R. Zeng, F. Tian, J. Yu, M. Dai, B. Niu, M. Li, L. Liu, R. Li, and Y. Liao, "Research on measuring methods and sensors of high voltage DC electric field," in *2014 International Conference on Information Science, Electronics and Electrical Engineering*, vol. 2, pp. 850–854, 2014.

[22] J. Chubb, "Two new designs of 'field mill' type fieldmeters not requiring earthing of rotating chopper," *IEEE Transactions on Industry Applications*, vol. 26, no. 6, pp. 1178–1181, 1990.

[23] B. Ling, C. Peng, R. Ren, Z. Chu, Z. Zhang, H. Lei, and S. Xia, "Design, fabrication and characterization of a MEMS-based three-dimensional electric field sensor with low cross-axis coupling interference," *Sensors*, vol. 18, no. 3, 2018.

[24] G. Gaborit, F. Lecoche, J. Dahdah, E. Duraz, L. Duvillaret, and J.-L. Lasserre, "Non-invasive vectorial electric field characterization with optical probes," in *2013 International Conference on Electromagnetics in Advanced Applications (ICEAA)*, pp. 1016–1019, 2013.

[25] K. S. Cover, *The fluxgate electric field meter A feasability study*. PhD thesis, University of British Columbia, 1986.

[26] B. Ando, S. Baglio, A. R. Bulsara, and V. Marletta, "A ferroelectric-capacitor-based approach to quasistatic electric field sensing," *IEEE Transactions on Instrumentation and Measurement*, vol. 59, no. 3, pp. 641–652, 2010.

[27] D. Robbes, "Sensor for non-contact electric field measurements," 03 2009. EP 2 040 086 A1.

[28] Y. Ohkuma, T. Ikeyama, and Y. Nogi, "Double-sensor method for detection of oscillating electric field," *Review of Scientific Instruments*, vol. 82, no. 4, p. 043501, 2011.

[29] L. Ichkitidze, N. Bazaev, D. Telyshev, R. Preobrazhensky, and M. Gavrushina, "Magnetic field sensors in medical diagnostics," *Biomedical Engineering*, vol. 48, pp. 305–309, 03 2015.

[30] J. Lenz and A. Edelstein, "Magnetic sensors and their applications," *Sensors Journal, IEEE*, vol. 6, pp. 631–649, 07 2006.

[31] O. Mareschal, B. Dufay, S. Lebargy, G. Allègre, M. Denoual, and D. Robbes, "Non conducting object detection using low frequency electric field imaging: Possible application to anomaly detection in insulating materials," in *2016 IEEE SENSORS*, pp. 1–3, 2016.

[32] D. Robbes, "Electric field generating device, electric field generating system, electric field detecting device, and electric field detection assembly," 2022. PCT/FR2022/050396.

[33] P. T. Metzger and J. Lane, "Electric potential due to a system of conducting spheres," *The Open Applied Physics Journal*, vol. 2, pp. 32–48, 2009.

[34] J. C. Maxwell, *A Treatise on Electricity and Magnetism*. Clarendon Press, 1873.

[35] B. Zitová and J. Flusser, "Image registration methods: a survey," *Image and vision computer*, vol. 21, pp. 977–1000, 2003.